Fault-Tolerant Operation of Six-Phase Energy Conversion Systems With Parallel Machine-Side Converters

Ignacio Gonzalez-Prieto, Mario J. Duran, H. S. Che, Emil Levi, *Fellow, IEEE*, Mario Bermúdez, and Federico Barrero, *Senior Member, IEEE*

***Abstract*—The fault tolerance provided by multiphase machines is one of the most attractive features for industry applications where a high degree of reliability is required. Aiming to take advantage of such postfault operating capability, some newly designed full-power energy conversion systems are selecting machines with more than three phases. Although the use of parallel converters is usual in high-power three-phase electrical drives, the fault tolerance of multiphase machines has been mainly considered with single supply from a multiphase converter. This study addresses the fault-tolerant capability of six-phase energy conversion systems supplied with parallel converters, deriving the current references and control strategy that need to be utilized to maximize torque/power production. Experimental results show that it is possible to increase the postfault rating of the system if some degree of imbalance in the current sharing between the two sets of three-phase windings is permitted.**

***Index Terms*—Fault tolerance, field-oriented control, multiphase energy conversion systems, parallel converters.**

I. Introduction

ENERGY conversion systems with full-power back-to-back (BTB) converters have recently gained popularity due to their capability to handle bidirectional power flow with a good controllability [1]. Compared to partial-power topologies using doubly fed induction generators (DFIGS), the higher degree of control provided by full-power configurations is currently appreciated in wind energy industry due to the tighter low-voltage ride through (LVRT) requirements of different grid codes [2], [3]. In addition, the BTB arrangement allows the control of both the power delivered to the machine and to the grid, and this can be useful in traction applications with regenerative braking. In this latter case, the machine operates as a motor but the BTB topology allows the system to transfer the decelerating kinetic energy into the grid.

Regardless of the application, the use of full-power BTB systems with an intermediate dc-link decouples the machine and grid sides, thus allowing the use of multiphase machines connected to three-phase grids [4]. Industrial examples of multiphase systems with full-power BTB converters are the 1.1 MW nine-phase permanent-magnet (PM) motor drive used in ultra-high-speed elevators [5] (motoring) and the 5 MW 12-phase PM synchronous generator used in wind energy turbines [6] (generation). The combination of different number of phases and converter arrangements results in multiple multiphase topologies, including the use of independent BTB three-phase modules [5], [6], the use of parallel three-phase converters [7], and the series connection of machine-side converters [8]–[11].

The literature on multiphase machines and drives points out different advantages over standard three-phase machines but maybe the most convincing one for industry is the capability to provide fault tolerance with no extra hardware [12], [13]. Among the different types of faults that may occur in a multiphase drive, the open-circuit faults (phase and line) have been the most widely studied cases because simple software reconfiguration suffices to obtain satisfactory postfault operation. When an n-phase machine is star connected and supplied by an n-phase converter, the open-circuit fault implies that the current can no longer flow through the faulted phase and the machine effectively has only $n-1$ phases located in an asymmetrical manner. In such situation, the fault needs to be firstly detected [14], [15] and then several modifications need to be done to obtain satisfactory postfault operation, including the recalculation of the current references [16], [17], the derating of the drive [18], and the use of specific control schemes [19]–[25]. A great body of knowledge has been recently reported in this field for different numbers of phases, using various machine and converter types [12]–[25], but considering single n-phase supply in all cases.

Nevertheless, the use of single voltage-source converters (VSCs) in high-current applications is not possible due to the limited rating of the IGBT-based converters. A good example can be found in the wind energy industry, where the use of low-voltage generators in high-power turbines ($\sim$10 MW) leads to the use of multiple parallel units [6]. Since redundant design is an effective solution to maintain postfault operation and to thus reduce the number of unexpected breakdowns of systems,

Manuscript received March 9, 2015; revised May 30, 2015; accepted June 30, 2015. Date of publication July 13, 2015; date of current version November 30, 2015. This work was supported by the Spanish Ministry of Science and Innovation under Project ENE2014-52536-C2–1-R and Project DPI2013-44278-R and the Junta de Andalucía under Project P11-TEP-7555. Recommended for publication by Associate Editor M. Liserre.

I. Gonzalez-Prieto, M. Bermúdez, and F. Barrero are with the Department of Electronic Engineering, University of Seville, 41004 Seville, Spain (e-mail: igonzalez14@us.es; mbermudez5@us.es; fbarrero@us.es).

M. J. Duran is with the Department of Electrical Engineering, University of Malaga, 29071 Malaga, Spain (e-mail: mjduran@uma.es).

H. S. Che is with the UMPEDAC, University of Malaya, 50603 Kuala Lumpur, Malaysia (e-mail: hsche@um.edu.my).

E. Levi is with the School of Engineering, Technology and Maritime Operations, Liverpool John Moores University, Merseyside, L3 5UA, U.K. (e-mail: e.levi@ljmu.ac.uk).

Color versions of one or more of the figures in this paper are available online at http://ieeexplore.ieee.org.

Digital Object Identifier 10.1109/TPEL.2015.2455595

various power converter topologies equipped with redundant capability are proposed in [26]. The use of parallel converters has been popular in three-phase energy conversion systems [1], where the single switch fault no longer implies that the current of the faulted phase is zero and all currents need to be derated to $(m-1)/m$ of the rated value if m parallel converters are operated. A similar concept can be extended to multiphase drives but further analysis is required [27], [28]. The redundancy obtained using six-phase induction machines and parallel converters has been recently addressed in [28], [29], where the enhancement of the fault-tolerant capability of energy conversion system has been studied by simulations. This study extends the analysis and includes experimental results that confirm the possibility to reduce the drive derating by allowing an unequal current sharing between the two sets of three-phase windings. The main contributions of this paper are:

1) The analysis of the fault tolerance of different multiphase topologies that include parallel converters.
   Previous investigations on the fault tolerance of multiphase machines have been focused on topologies with single VSC supply, where converter faults lead to open-phase faults. This implies in turn that topologies with independent dc links [5], [6] need to disable the set of windings supplied by the faulty converter, whereas topologies with series connection of VSCs [8]–[11] cannot continue operating. The situation differs in the scenario considered in this study because single converter faults only imply a reduction in the per-phase current. To fully exploit the fault-tolerant capability of the system the machine needs to be asymmetrically operated, this being addressed for the first time in this paper.
2) The derivation of the *x–y* current references to permit the unbalanced operation of the drive.
   Although the balanced operation resulting from the operation with zero *x–y* currents maximizes efficiency, the drive derating in postfault situation can only be reduced by allowing the injection of nonzero *x–y* currents in certain manner to comply with the postfault current restrictions. This study determines the *x–y* current waveforms that are required to maximize the achievable torque and also defines the most appropriate reference frame for *x–y* currents to ease the design of the current controllers.
3) The proposal of an additional controller to dynamically regulate the postfault currents.

The asymmetrical current sharing between the multiphase machine windings, discussed in 1) and determined in 2), should be variable in order to maximize the postfault efficiency. In other words, the *x–y* currents should be injected only when needed to avoid the appearance of extra copper losses. For this purpose, this study suggests the use of an additional controller that regulates the degree of imbalance and optimizes the current sharing between windings.

The paper is organized as follows. Section II describes different multiphase topologies that use parallel converters and analyzes their fault-tolerant capability. The postfault system capability is quantified in Section III, where an imbalance in the current sharing of the two sets of three-phase windings is assumed. A new controller to allow imbalance in the multiphase system is proposed in Section IV, and the fault-tolerant capability of the system is experimentally studied in Section V where steady-state and dynamic tests are shown for healthy (prefault) and postfault scenarios. Conclusions are finally summarized in the last section.

II. Six-Phase Energy Conversion Systems' Topologies

Six-phase energy conversion systems are normally based on asymmetrical dual three-phase induction machines with two isolated neutrals. This six-phase machine is a continuous system that can be described by a set of differential equations that can be simplified in stationary coordinates using the vector space decomposition (VSD) approach [30]. Using VSD, the original six-dimensional space of the machine is transformed into three two-dimensional orthogonal subspaces usually denoted as $\alpha-\beta$, $x-y$, and 0_+-0_-, where only $\alpha-\beta$ components contribute to the flux and torque production. The $\alpha-\beta$ components represent the fundamental supply component plus supply harmonics of the order $12n\pm1$ ($n=1,2,3,1/4$). The second stator–rotor pair of components represents supply harmonics of the order $6n\pm1$ ($x-y$ subspace with $n=1,3,5,1/4$), while the zero-sequence harmonic components can exist only if there is a single neutral point, in which case they belong to the third pair of components. The asymmetrical six-phase induction machine model, obtained using VSD and the standard assumptions of the ac machine modeling (negligible iron losses, space harmonics, and magnetic saturation), can be summarized as follows:

$$
\begin{aligned}
v_{\alpha s} &= \left(R_s + L_s\cdot\frac{d}{dt}\right)\cdot i_{\alpha s} + M\cdot\frac{d}{dt}i_{\alpha r}\\
v_{\beta s} &= \left(R_s + L_s\cdot\frac{d}{dt}\right)\cdot i_{\beta s} + M\cdot\frac{d}{dt}i_{\beta r}\\
v_{xs} &= \left(R_s + L_{ls}\cdot\frac{d}{dt}\right)\cdot i_{xs}\\
v_{ys} &= \left(R_s + L_{ls}\cdot\frac{d}{dt}\right)\cdot i_{ys}\\
0 &= \left(R_r + L_r\cdot\frac{d}{dt}\right)i_{\alpha r} + \omega_r\cdot L_r\cdot i_{\beta r} + M\cdot\frac{d}{dt}i_{\alpha s}\\
&\quad + \omega_r\cdot M\cdot i_{\beta s}\\
0 &= \left(R_r + L_r\cdot\frac{d}{dt}\right)i_{\beta r} - \omega_r\cdot L_r\cdot i_{\alpha r} + M\cdot\frac{d}{dt}i_{\beta s}\\
&\quad - \omega_r\cdot M\cdot i_{\alpha s}
\end{aligned}
\tag{1}
$$

where $L_s = L_{ls}+3L_{ms}$, $L_r = L_{lr}+3L_{ms}$, $M=3L_{ms}$, ω_r is the rotor electrical speed ($\omega_r = p\cdot\omega$, p being the pole pair number), indices s and r denote stator and rotor variables, respectively, and subscripts $l$and m indicate leakage and magnetizing inductance, respectively.

Model (1) can be used to study the performance of the machine during the healthy and faulty operation of the entire system. In healthy operation (neglecting switching and dead-time harmonics), only $\alpha-\beta$ components will exist. The additional

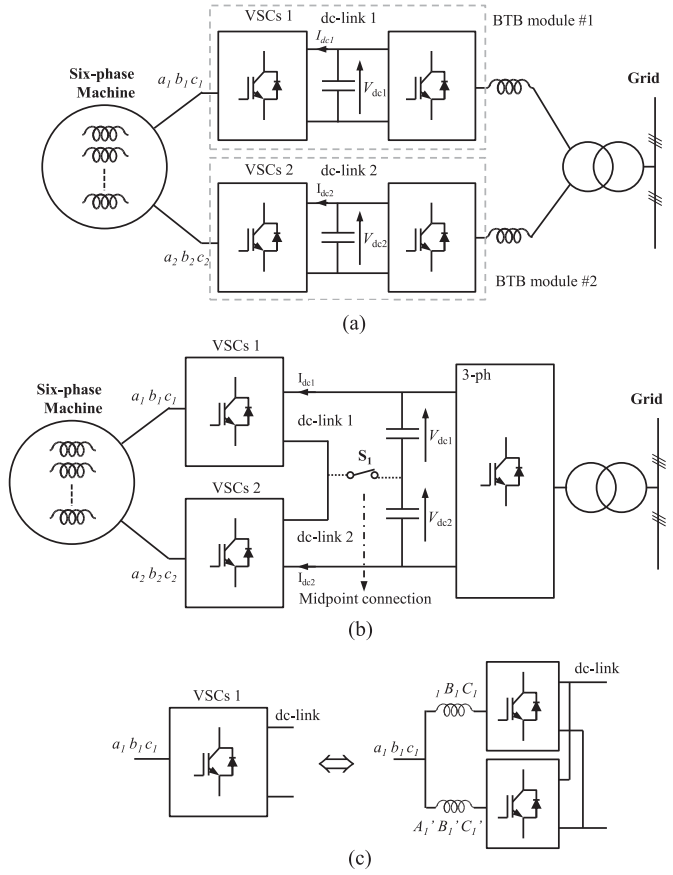

Fig. 1. Multiphase energy conversion topologies: (a) independent BTB VSC modules, (b) series connection of VSCs, and (c) parallel connection of VSCs.

degrees of freedom that become available for control purposes during the faulty operation are related to the $x-y$ subspace components, provided that the converter topology allows for this functionality.

Different topologies for six-phase energy conversion systems with fault-tolerant capability have been recently analyzed by the scientific community. The first topology uses independent BTB three-phase modules, each one supplying a different set of three-phase windings [see Fig. 1(a)]. Such an option has been industrially implemented both in traction and wind energy applications using 9-, 12-, and 18-phase machines supplied from three, four, and six BTB three-phase modules, respectively [5], [6], [31]. This topology has a simple and modular structure and is a natural extension of the standard three-phase case. From the fault tolerance point of view, this arrangement allows postfault operation in the event of a fault either in the machine, converter, or dc link. The procedure to obtain postfault operation under single open-circuit fault is simple: the whole three-phase BTB faulted module is disconnected and the machine operates with the remaining healthy modules. For the specific case of a six-phase machine this strategy is termed 'single VSC', and it implies that the postfault α–β current capability is 50% after single open-circuit fault [7], resulting in only 25% of prefault torque/power for given slip and frequency.

A second option is to cascade the machine-side converters and connect the dc-link to a grid-side converter [see Fig. 1(b)], which can be multilevel in order to reduce the voltage stress of the IGBTs and improve the current quality [8]. The main idea is to maintain low voltage on the machine-side but elevate the dc-link voltage to allow medium voltage at the grid side [9]–[11]. This, in turn, reduces the current rating and the cable size for the given power, hence giving a potential overall capital cost reduction. This cascaded topology is particularly suitable for multi-MW wind energy applications, because the generators typically operate at low-voltage while the medium voltage on the grid-side allows transformerless generation [9], [10]. The machine side may have a dc-link midpoint connection to the grid side [S_1 closed in Fig. 1(b)] or leave the dc-link midpoint isolated [S_1 open in Fig. 1(b)]. The latter case allows a two-wire connection between machine and grid sides, which can be advantageous in the case of off-shore wind farms [4], but requires an additional controller of the *x–y* currents to regulate the midpoint voltage [9]. If the dc-link midpoint is not isolated, the voltage balancing task can be performed from the grid side, although the *x–y* controller in the machine side is still desirable to improve the system dynamics [32].

In spite of the advantage of the series connection to generate at medium voltage, from the point of view of the fault tolerance the postfault operation is no longer possible with the cascaded structure shown in Fig. 1(b). The reason is that the six-phase machine needs to be operated using two isolated neutrals (to prevent the flow of zero-sequence currents) and the open-circuit implies that the faulted set becomes single phase. Although the healthy set of three-phase windings can still deliver rated current, it is not possible to balance the dc-link voltages [V_{dc1} and V_{dc2} in Fig. 1(b)] anymore because of the power oscillations caused by the single-phase (i.e., faulted) set.

To summarize, the use of independent BTB modules provides limited fault-tolerant capability (25% of prefault torque/power for given slip and frequency), whereas the series connection of the VSCs has no fault-tolerant capability at all. This scenario can be improved if the six-phase machine is fed by four three-phase two-level VSCs. In other words, each set of three-phase windings is connected to two three-phase VSCs operating in parallel [see Fig. 1(c)]. Interfacing inductors are placed at the output of each VSC to facilitate parallel operation of the two VSCs. For the purpose of the discussion that follows, it is assumed that the set of windings $a_1b_1c_1$ is connected to VSCs $A_1B_1C_1$ and $A_1'B_1'C_1'$ (collectively termed as VSCs1), and the set of windings $a_2b_2c_2$ is connected to VSCs $A_2B_2C_2$ and $A_2'B_2'C_2'$ (collectively termed as VSCs2). Due to the parallel connection, the phase current is shared between the two VSCs, so that each VSC only needs to be sized to take half of the rated phase current. This reduction in the per VSC current is adequate in low-voltage high-power drives, where the use of only two VSCs to drive the six-phase machine is not feasible due to the limited ratings of IGBT-based VSCs (typically around 1 MW). In addition, the redundancy provided by the parallel converters provides enhanced fault tolerance. Similarly to the case of three-phase generators, the parallel converters [see Fig. 1(c)]

are not tolerant to winding open-phase faults but they provide additional fault tolerance against converter faults, which are more common and unpredictable than machine faults [4].

The dc links of VSCs1 and VSCs2 can then be kept independent [see Fig. 1(a)] or be cascaded in series to form an elevated dc-link voltage [see Fig. 1(b)]. In the latter case the topology results in a hybrid series–parallel topology similar to the one suggested in [27]–[29], and the merits are in between that of a pure series and pure parallel connection: elevated dc-link voltage with some degree of fault tolerance. Additional features of the topologies of Fig. 1(a) and (b) include lower *dv*/*dt* of the common-mode voltage (CMV), which is known to be a main cause of leakage currents in high power applications and lower voltage rating of the power converters. In any case, the most relevant characteristic, compared to the case of single VSC supply, is the improved fault tolerant capability, which is explored next.

III. Postfault System Capability

The case of a single open-circuit fault is analyzed hereafter, where one of the converter legs is disconnected from the machine winding due to a fault. Without lack of generality, it is assumed further on that leg A_1' of the VSCs1 is faulted. Due to the parallel connection of the converters $A_1B_1C_1$ and $A_1'B_1'C_1'$, phase a_1 is still fed with leg A_1 of VSCs1, and consequently, the current can still flow. However, maximum phase current i_{a1} is now just half of the rated phase current due to the limitation on the VSCs current rating.

In the study of the system capability, it is first assumed that the oscillation of the dc-link voltage in not permissible. To ensure nonoscillating dc-link voltage, the active power flowing in each of the two sets of three-phase windings should be constant. Since the machine is not damaged by the fault, this implies that the three-phase currents (either in VSCs1 or VSCs2) need to be balanced, i.e., with same amplitudes and 120° of phase shift. The current amplitudes of VSCs1 are limited to half the rated value due to the limitation on the faulted phase, so the maximum steady-state currents are

$$\begin{aligned} i_{a1} &= 0.5 \cdot I_n \cdot \cos(\omega \cdot t) \\ i_{b1} &= 0.5 \cdot I_n \cdot \cos(\omega \cdot t - 120^\circ) \\ i_{c1} &= 0.5 \cdot I_n \cdot \cos(\omega \cdot t - 240^\circ) \end{aligned} \tag{2}$$

where ω is the angular frequency of stator phase currents and I_n is the peak value of the rated current.

For the same reason of avoiding oscillating power, the phase currents in winding 2 should also have the same magnitude and 120° of phase separation. However, since the VSCs2 remain healthy, the current in each winding can go up to the rated value. To represent a general case that facilitates further study, the phase currents can be written as

$$\begin{aligned} i_{a2} &= k \cdot I_n \cdot \cos(\omega \cdot t - 30^\circ) \\ i_{b2} &= k \cdot I_n \cdot \cos(\omega \cdot t - 150^\circ) \\ i_{c2} &= k \cdot I_n \cdot \cos(\omega \cdot t - 270^\circ) \end{aligned} \tag{3}$$

where k represents a constant $0 < k < 1$, which can be optimized.

By applying the power-invariant Clarke decoupling transformation [6]

$$[T] = \frac{1}{\sqrt{3}} \begin{bmatrix} 1 & -1/2 & -1/2 & \sqrt{3}/2 & -\sqrt{3}/2 & 0 \\ 0 & \sqrt{3}/2 & -\sqrt{3}/2 & 1/2 & 1/2 & -1 \\ 1 & -1/2 & -1/2 & -\sqrt{3}/2 & \sqrt{3}/2 & 0 \\ 0 & -\sqrt{3}/2 & \sqrt{3}/2 & 1/2 & 1/2 & -1 \end{bmatrix} \tag{4}$$

to the phase currents of (2) and (3), the stator α–β and *x*–*y* currents can be0 obtained

$$\begin{aligned} i_{\alpha s} &= \sqrt{3} \cdot I_n \cdot (0.25 + 0.5 \cdot k) \cdot \cos(\omega \cdot t) \\ i_{\beta s} &= \sqrt{3} \cdot I_n \cdot (0.25 + 0.5 \cdot k) \cdot \sin(\omega \cdot t) \\ i_{xs} &= \sqrt{3} \cdot I_n \cdot (0.25 - 0.5 \cdot k) \cdot \cos(\omega \cdot t) \\ i_{ys} &= \sqrt{3} \cdot I_n \cdot (-0.25 + 0.5 \cdot k) \cdot \sin(\omega \cdot t). \end{aligned} \tag{5}$$

Zero-sequence currents are omitted from the analysis because the machine is configured with two isolated neutral points that prevent their flow.

Since currents in both windings are a set of balanced three-phase currents, *x*–*y* currents are related to α–β currents by the *k* factor

$$i_{xs} = \frac{0.5 - k}{0.5 + k} i_{\alpha s}, \quad i_{ys} = -\frac{0.5 - k}{0.5 + k} i_{\beta s}. \tag{6}$$

This means that *x*–*y* currents have the same frequency and phase relation as the α–β currents, with the difference only in their amplitudes. The relationship derived in (6) is important for control purposes and will be used in Section IV to build a controller that permits the unbalanced operation defined in (2) and (3) with $k > 0.5$.

From (5), it can be observed that the α–β current magnitude increases with the value of *k*. This implies that increasing *k* will increase the flux and torque, which, in turn, increases the torque/power. Nevertheless, changing the value of *k* will also cause the flow of *x*–*y* currents, which introduces additional copper losses in the stator windings and reduces the actual torque/power obtained from the machine. No distortion of the airgap flux and torque are expected by the appearance of *x*–*y* currents because the six-phase induction generator is considered to have distributed windings, and consequently, spatial harmonics are negligible.

For the specific case of $k = 0.5$, all phase currents form a balanced set of asymmetrical six-phase signals with amplitudes of $I_n/2$. Since the currents are balanced, *x*–*y* currents are zero. Even though this strategy minimizes losses by having zero *x*–*y* currents, the maximum α–β current magnitude is only half of the rated value, which diminishes the maximum achievable power.

In order to analyze the steady-state achievable power for increasing values of *k*, the currents can be expressed in complex

form as

$$\begin{aligned} i_{\alpha\beta s} &= (i_{\alpha s} + j \cdot i_{\beta s}) \\ i_{xys} &= (i_{xs} + j \cdot i_{ys}) \\ i_{\alpha\beta r} &= (i_{\alpha r} + j \cdot i_{\beta r}). \end{aligned} \tag{7}$$

From the equivalent circuit of a squirrel-cage induction machine [28], it is possible to calculate the power balance and obtain the output power (neglecting mechanical and iron losses)

$$\begin{aligned} P_{\text{out}} &= P_{\text{in}} - P_{\text{Cu}-\alpha\beta r} - P_{\text{Cu}-\alpha\beta s} - P_{\text{Cu}-xys} \\ P_{\text{out}} &= \frac{1-s}{s} \cdot R_r \cdot |i_{\alpha\beta r}|^2 \quad P_{\text{Cu}-\alpha\beta r} = R_r \cdot |i_{\alpha\beta r}|^2 \\ P_{\text{Cu}-\alpha\beta s} &= R_S \cdot |i_{\alpha\beta s}|^2 \qquad P_{\text{Cu}-xys} = R_S \cdot |i_{xys}|^2 \end{aligned} \tag{8}$$

where stator and rotor currents are those defined in (7). P_{in} is the power provided by the prime mover (generator) or the electrical supply (motor). P_{out} is the electrical power generated by the system (generator) or the mechanical power on the shaft (motor), and P_{Cu} are the copper losses associated with the different currents flowing in the machine. From the equivalent circuit [28] and (5), the rotor α–β rotor currents can be expressed as a function of the parameter *k*

$$|i_{\alpha\beta r}| = \frac{\sqrt{3} \cdot X_m \cdot (0.5 \cdot k + 0.25) \cdot I_n}{\sqrt{(X_m + X_{lr})^2 + \left(\frac{R_r}{s}\right)^2}}. \tag{9}$$

Postfault torque/power with $k = 0.5$ is 25% (similarly to the case with single VSC supply) of the prefault value for a given slip and frequency, as it could be expected because the α–β currents are half of the prefault value and torque/power increases with the square of the current ($0.5^2 = 0.25$). Similarly, postfault torque/power with $k = 1$ (maximum value of *k* with parallel VSC supply) is 56.25% of the prefault generated power. This is again expected since the α–β currents are 75% of the prefault value ($0.75^2 = 0.5625$). Consequently, for the same frequency and slip, increasing the value of *k* elevates the achievable torque/power by 225% ($56.25/25 = 2.25$) compared to single VSC supply, if a proper imbalance strategy is designed for the parallel connection of Fig. 1(c). In a general case, the slip and frequency do not remain constant and the achievable power depends on the ratio of the *d*–*q* reference currents (i_{ds}/i_{qs}) [7], [29]. In any case, the steady-state analysis shows that the capability to increase the α–β currents results in a relevant gain of the postfault achievable torque/power.

All the analysis developed so far is common to the topologies of Fig. 1(a) and (b) because the current control is not affected by the arrangement of the individual dc links. Nevertheless, the imbalance that results from operating the drive with $k > 0.5$ has a different impact on the dc-link voltages of independent and cascaded topologies. In the case of Fig. 1(a) the power extracted from dc links 1 and 2 is different in postfault operation ($P_1 \neq P_2$), but the dc currents can also be different ($I_{\text{dc1}} \neq I_{\text{dc2}}$), allowing unbalanced current operation with constant dc-link voltages ($V_{\text{dc1}} = V_{\text{dc2}}$). Nevertheless, in the case of the cascaded topology of Fig. 1(b) with no dc-link midpoint connection to the grid-side [S_1 open in Fig. 1(b)], the dc currents are forced to be equal ($I_{\text{dc1}} = I_{\text{dc2}}$), causing an imbalance in the dc-link voltages

$$\frac{V_{\text{dc1}}}{V_{\text{dc2}}} = \frac{I_{\text{dc2}}}{I_{\text{dc1}}} \cdot \frac{P_1}{P_2} < 1. \tag{10}$$

The degree of dc-link voltage imbalance depends on the current imbalance, defined by *k*, and the machine impedances. Further details and an analytical derivation can be found in [29]. The voltage imbalance can be solved in the cascaded topology if the dc-link midpoint is connected to the grid side [S_1 closed in Fig. 1(b)], because the restriction $I_{\text{dc1}} = I_{\text{dc2}}$ does not apply in this case.

IV. Proposed Fault-Tolerant Controller

The general structure of the prefault control strategy is shown in Fig. 2. The scheme is an indirect rotor field-oriented control (IRFOC) with an outer speed loop and inner current loops for *d*–*q* and *x*–*y* currents. Only four phase currents (i_{a1}, i_{b1}, i_{a2}, and i_{b2}) need to be measured because the remaining phase currents can be obtained from the condition of having two isolated neutral points. Measured phase currents are converted into α–β currents using the Clarke transformation $[T]$ of (4) and *d*–*q* currents are obtained from the rotation of α–β currents in the forward (synchronous) direction using the Park transformation

$$[D] = \begin{bmatrix} \cos\theta_s & \sin\theta_s \\ -\sin\theta_s & \cos\theta_s \end{bmatrix} \tag{11}$$

where the angle θ_s of the rotating reference frame is obtained from the measured speed ω and the estimated slip

$$\theta_s = \int \left(\frac{i_{qs}^*}{T_r i_{ds}^*} + P \cdot \omega \right) dt \tag{12}$$

where *P* is the number of pole pairs and T_r is the rotor time constant.

The machine is fluxed by setting a value of i_{ds}^* that corresponds to the rated flux of the machine, while the torque is regulated by the outer speed control loop that provides the reference of the quadrature current i_{qs}^*. The output of the *d*–*q* current controllers and the decoupling terms e_{ds} and e_{qs} [12] provide the reference voltages v_{ds}^* and v_{qs}^*.

The second inner current-control loop corresponds to the *x*–*y* current components. Control can be performed in the stationary reference frame using the Clarke transformation $[T]$, in the synchronous frame using the Park transformation $[D]$, or in the antisynchronous frame using the inverse of the Park transformation $[D]^{-1}$ [33]

$$[D]^{-1} = \begin{bmatrix} \cos\theta_s & -\sin\theta_s \\ \sin\theta_s & \cos\theta_s \end{bmatrix}. \tag{13}$$

In the prefault situation, and considering the independent BTB topology of Fig. 1(a), the *x*′–*y*′ current references $i_{xs}'^*$ and $i_{ys}'^*$ are zero [see Fig. 2(a)] and the *x*–*y* current control can still be performed in the stationary frame. However, for the cascaded topology of Fig. 1(b), $i_{ys}'^*$ is obtained from a dc-link voltage balancing controller [see Fig. 2(b)] that ensures similar V_{dc1} and V_{dc2} values by proper injection of *y*′ current to

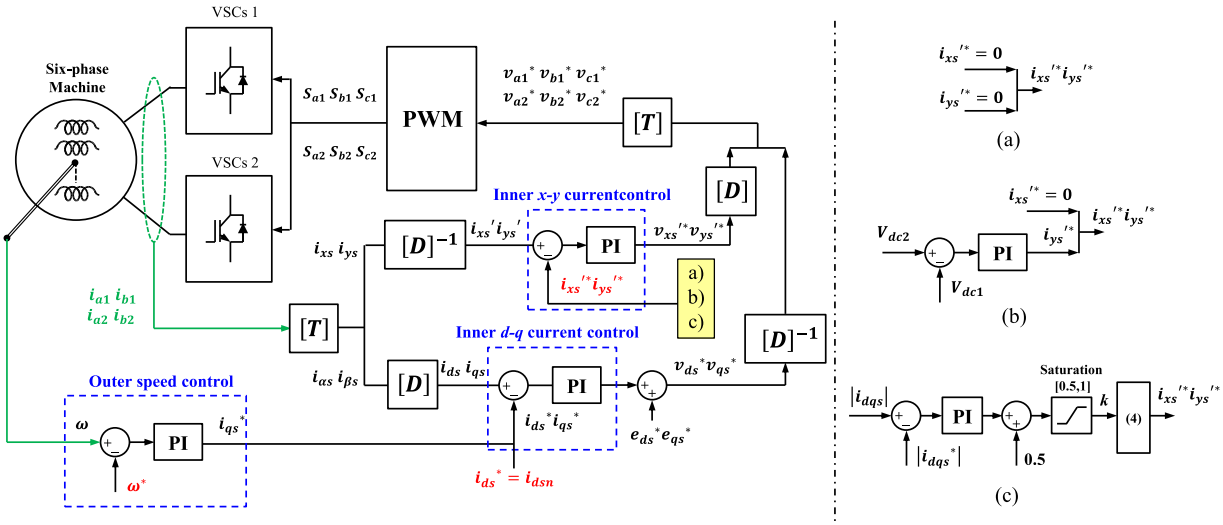

Fig. 2. FOC of the six-phase induction machine with synchronous d–q current control and antisynchronous x–y current control (left) and x'–y' current reference calculation (right) in (a) prefault situation with independent BTB topology [see Fig. 1(a)], (b) prefault situation with cascaded topology [see Fig. 1(b)], and (c) postfault condition for either independent BTB or cascaded topologies. Applies to the case of paralleled converters for each three-phase winding at the machine's side.

divert the active power from VSCs1 to VSCs2 or vice versa [9]. In this case, the x–y current components need to be rotated in the antisynchronous direction [33] (termed i'_{xs}, i'_{ys} in Fig. 2) to facilitate the control of the active power from the y-current-control loop, the output of the x–y current controllers provides the x'–y' voltage references v'^{*}_{xs} and v'^{*}_{ys} in antisynchronous reference frame, and the d–q and $x'-y'$ reference voltages are transformed in the inverse direction using the Park ($[D]$and $[D]^{-1}$) and Clarke ($[T]$) matrices to provide the phase voltage references ($v^{*}_{a1}v^{*}_{b1}v^{*}_{c1}v^{*}_{a2}v^{*}_{b2}v^{*}_{c2}$), which are inputs for the carrier-based six-phase PWM [7], [9] that generates the switching signals to VSCs1 and VSCs2.

The aim in postfault situation is to drive the machine ensuring that the currents in the faulted VSCs1 are below half the rated value ($\max|i_{a1b1c1}| \leq I_n/2$). This target can be achieved by using a constant degree of imbalance (e.g., setting $k=1$ for all operating points), but this results in a suboptimal solution because efficiency would be decreased due to unnecessary injection of x–y currents. In the low-torque region, for example, the limit of VSCs1 is not reached and consequently the machine can be symmetrically operated as in prefault situation [see Fig. 2(a) or (b)] with no need to set $k>1$ and generate additional copper losses. However, when the torque is such that the currents in VSCs1 reach the postfault limit ($\max|i_{a1b1c1}| = I_n/2$) for $k=0.5$, the system can no longer increase the generated torque/power unless some imbalance in the power sharing of VSCs1 and VSCs2 is permitted. At this moment, the controller of Fig. 2(c) is activated. This controller is devised to provide variable x–y current injection (i.e., variable k) to generate only the minimum degree of imbalance that is required to comply with current limits. The designed strategy in turn favors the efficient operation by minimizing copper losses and also limits the imbalance in the dc-link voltages of cascaded topologies. The controller that regulates the imbalance is developed so that when the modulus of the d–q currents is above half the rated value, this excess is taken as the input for a proportional- integral (PI) anti-wind-up controller whose output is the k parameter. As the load torque increases, more q-current is required and a higher value of k is demanded. According to (6), the value of k determines the amount of x–y currents that need to be injected, in order to provoke the required imbalance of the system.

Nevertheless, it is important not only to determine the optimal amount of x–y currents but also to select a proper reference frame to simplify the control scheme. If the x–y control is performed in the stationary reference frame, as it is a common practice in multiphase drives in healthy operation [34], it is necessary to regulate sinusoidal currents and the limited bandwidth of PI controllers will result in a poor performance [33]. For the purpose of regulating varying x–y currents it has been recently suggested to use dual PI or resonant controllers [35], [36]; this, however, complicates to some extent the controller structure and tuning. Fortunately, in this case, it is possible to perform the control in a reference frame where x–y currents become constant. It can be noted from (6) that the required x-current is proportional to α-current while the required y-current is inversely proportional to the β-current. This implies that the α–β current vector rotates in synchronous direction whereas the x–y current vector rotates in antisynchronous direction. It follows that the rotation of x–y currents in backward direction leads to x–y currents (termed x'–y' in the rotating reference frame) becoming proportional to d–q currents

$$i_{xs'} = \frac{0.5-k}{0.5+k} i_{ds}, \qquad i_{ys'} = -\frac{0.5-k}{0.5+k} i_{qs}. \tag{14}$$

Consequently, the choice of this antisynchronous reference frame provides constant x'–y' references from (14) that allow the use of standard PI controllers. The use of resonant controllers (PR), which is a common procedure in fault-tolerant control

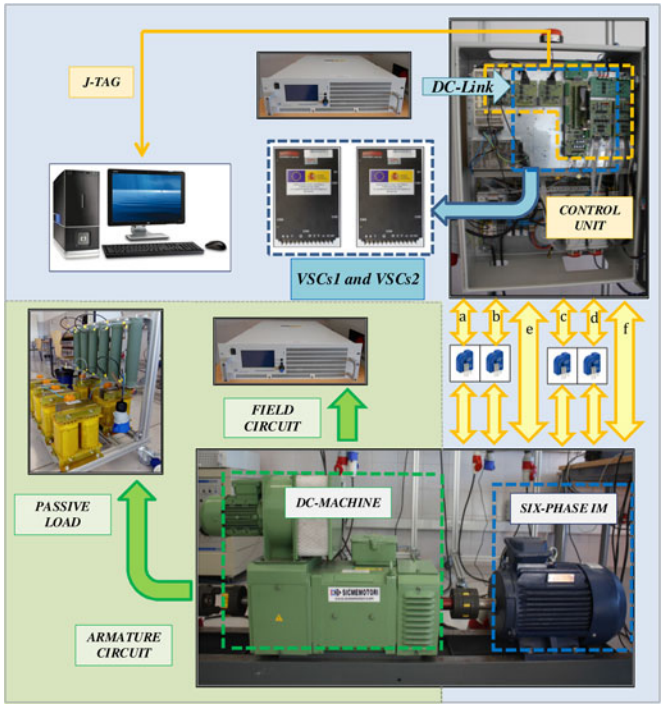

Fig. 3. Test bench used for the experimental results.

schemes with time-varying x–y current references [7], [21], [36], is then not necessary.

In the case of independent topologies of Fig. 1(a), the value of k is saturated to 1 to ensure that the maximum current of the healthy VSCs2 corresponds to the rated current, and the same applies to the cascaded topology with dc-link midpoint connection [S_1 in Fig. 1(b)]. When the dc-link midpoint of the cascaded topology is isolated, the value of k may be set to a lower value in the range [0.5,1], depending on the permissible dc-link voltage imbalance due to the ratings of the system (IGBTs and dc-link capacitor voltage capability) [29]. For the purpose of analysis, in this study, it is assumed that k can go up to 1, so that the maximum degree of unbalance is obtained.

V. Experimental Results

To evaluate the properties of the proposed fault-tolerant controller, it has been implemented in a laboratory-scale prototype. The test bench and experimental results are presented next.

A. Test Bench

A three-phase induction machine has been rewound to obtain the asymmetrical six-phase induction machine, shown within the test bench illustration in Fig. 3. Parameters of the custom-built six-phase machine have been determined using conventional, ac time domain and stand-still tests with inverter supply [37], [38], providing stator and rotor resistances of 4.2 and 2 Ω, stator and rotor leakage inductances of 4.2 and 55 mH, and mutual inductance of 420 mH. The six-phase machine is driven by conventional three-phase power converters from Semikron (SKS22F modules) that correspond to VSCs1 and VSCs2 in Fig. 1. The converters are connected to a dc power supply system as in Fig. 1(a), and the control actions are performed by a TI TMS320F28335 digital signal processor. The control unit is programmed through JTAG and TI proprietary software Code Composer Studio. Current and speed measurements are taken with four hall-effect LEM LAH 25-NP sensors and a GHM510296R/2500 digital encoder, respectively. The load torque is provided by a dc-machine whose armature is connected to a variable resistive–inductive load. The full scheme of the test bench is depicted in Fig. 3.

B. Experimental Results

Different experimental tests have been applied setting a flux reference $i_{ds}^{*} = 1$ A, a rated q current of 8 A, a switching frequency of 10 kHz, and dc-link voltages of $V_{\mathrm{dc1}} = V_{\mathrm{dc2}} = 300$ V. The threshold for the activation of the controller in Fig. 2(c) is set to $|i_{dqs}| = 4$ A, which corresponds to half the rated value. The transition from pre- to postfault situation is first tested to verify the capability of the system to withstand an open-circuit fault in leg A_1' of the VSCs1. The system is operated in prefault situation using the proposed control scheme with 62.5% of the rated current ($i_{qs}^{*} = 5$ A) and a reference speed $\omega^{*} = 800$ r/min [see Fig. 4(a)]. During the prefault situation (until $t = 10$ s), the value of k is 0.5 [see Fig. 4(b)], indicating an equal current sharing in both sets of three-phase windings (a_1, b_1, c_1 and a_2, b_2, c_2). According to (6), this implies that the x–y current references are set to zero ($i_{xs}'^{*} = i'*_{ys} = 0$) as indicated in the strategy of Fig. 2(a). To reach the balanced operation observed in Fig. 4(e), x–y currents are regulated to zero as shown in Fig. 4(d). Consequently, the prefault phase currents of the two sets of three-phase windings have equal amplitudes and a phase shifting of 30°. The d–q currents, responsible for the torque production, are successfully controlled to their reference values [see Fig. 4(c)], and this, in turn, implies that the machine speed is regulated to the reference speed [see Fig. 4(a)]. Now, when the fault occurs ($t = 10$ s), the x'–y' references are no longer set to zero but obtained from the controller shown in Fig. 2(c). Since the modulus of the d–q currents is over the threshold value ($|i_{dqs}| = 4$ A), k is quickly increased by the controller, as it can be observed in Fig. 4(b). The new value of k implies that x'–y' references are no longer set to zero but to values that are proportional to d–q current references (14). In our case, x'–y' currents track new nonzero references [see Fig. 4(d)], forcing the imbalance in the phase currents depicted in Fig. 4(e). Notice that the antisynchronous reference frame selected for the x'–y' components results in constant current reference values in the postfault situation, favoring the tracking process using PI controllers. Notice also that the unbalanced operation in postfault situation is characterized by a reduction (an increase, respectively) in the phase current of the faulty (healthy) three-phase winding (a_1, b_1, c_1 and a_2, b_2, c_2, respectively). Then, postfault d–q currents are maintained at their respective prefault references [see Fig. 4(c)] and the machine speed is regulated to the reference value [see Fig. 4(a)]. The transition from pre- to postfault operation is done without any impact on the d–q currents or the motor speed, this being one of the benefits of

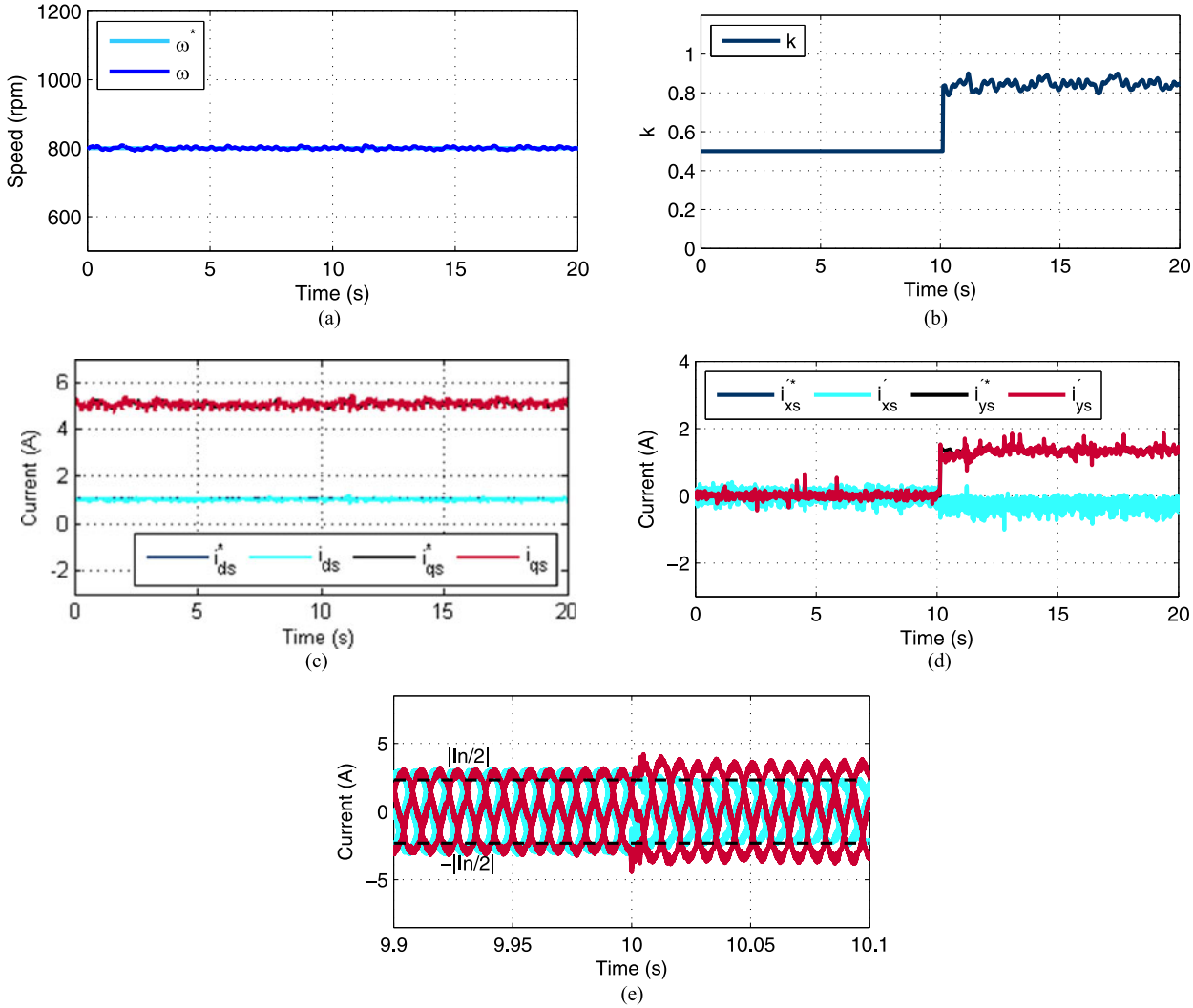

Fig. 4. Experimental results in the pre- to postfault transition at 800 r/min. From top to bottom: motor speed, degree of unbalance k, d–q currents, $x' - y'$ currents, and phase currents.

the proposed controller that regulates the unbalanced operation between three-phase windings.

The ability of the entire system to operate in postfault situation is a second benefit of the proposed unbalanced operation controller. In the case of balanced postfault operation ($k = 0.5$), the maximum q-current is $i^*_{qs} = 3.9$ A, indicating an insufficient current production to maintain the machine speed after the fault. The conclusions obtained from this test can be summarized as follows: 1) the proposed postfault x–y current references result in an unbalanced operation that allows preserving the post fault current ratings ($\max|i_{a1b1c1}| \leq I_n/2$ and $\max|i_{a2b2c2}| \leq I_n$); 2) the nonzero x'–y' current references in postfault situation are tracked by simple PI controllers due to the selected anti-synchronous reference frame that results in constant x'–y' current values; and 3) the transition from the pre- to the postfault situation is smoothly performed, and iv) higher d–q currents are obtained using the unbalanced operation, which allows maintaining the prefault drive performance in a wider range of operation.

Postfault operation is analyzed next using the proposed controller in steady and transient states. Fig. 5 shows the prefault performance with a change in the speed reference from 800 to 600 r/min at $t = 14$ s. Since the load torque is provided by a dc-machine whose power/torque is proportional to the square of the speed, the deceleration implies a reduction of the load torque. The q-current is decreased accordingly [see Fig. 5(b)] and the motor speed follows its reference value [see Fig. 5(a)]. The d-current is satisfactorily kept close to 1 A during the whole test and the x'–y' currents are driven to zero by the prefault controller.

The same test is repeated but with a fault instigated at $t = 10$ s (see Fig. 6). The imbalance is then regulated by the controller of Fig. 2(c), causing an increase of k up to approximately 0.82 after the fault occurrence [see Fig. 6(d)]. Since the modulus of the d–q currents is reduced during the transient, the value of k is also reduced because a lower degree of imbalance is required at 600 r/min. Compared to the healthy case shown in Fig. 5, the motor speed [see Fig. 6(a)] and d–q currents [see Fig. 6(b)]

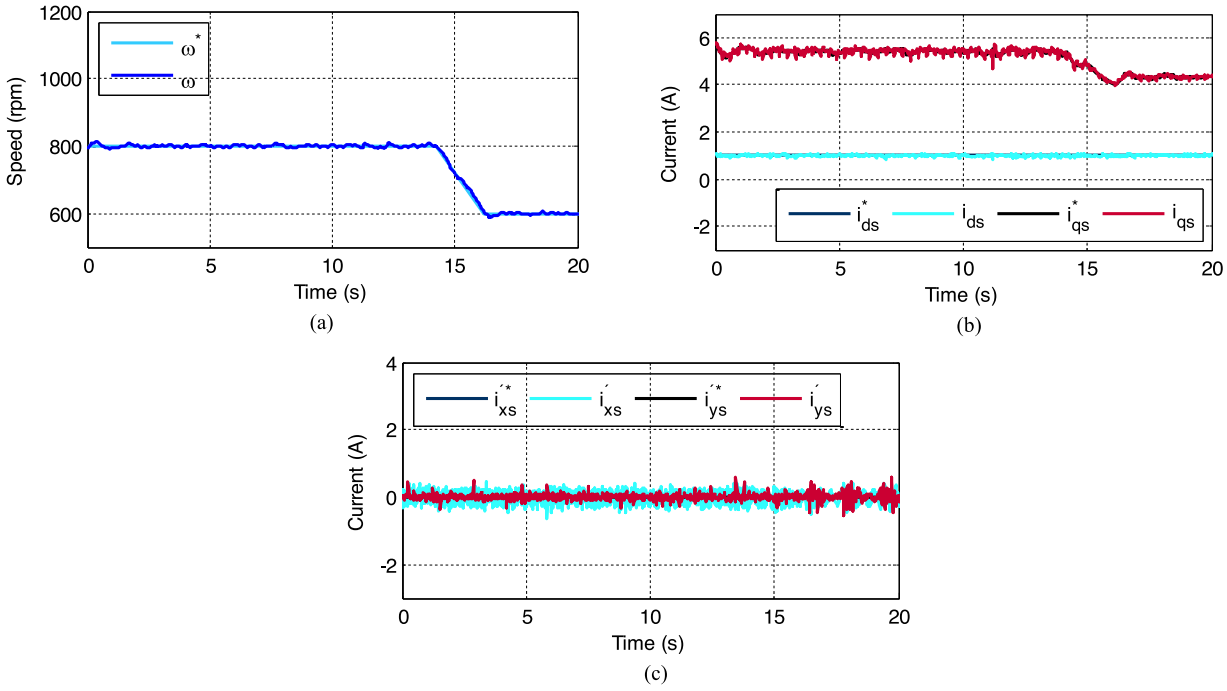

Fig. 5. Experimental results in the test with a speed change from 800 to 600 r/min (prefault). From top to bottom: motor speed, d–q currents, and $x' - y'$ currents.

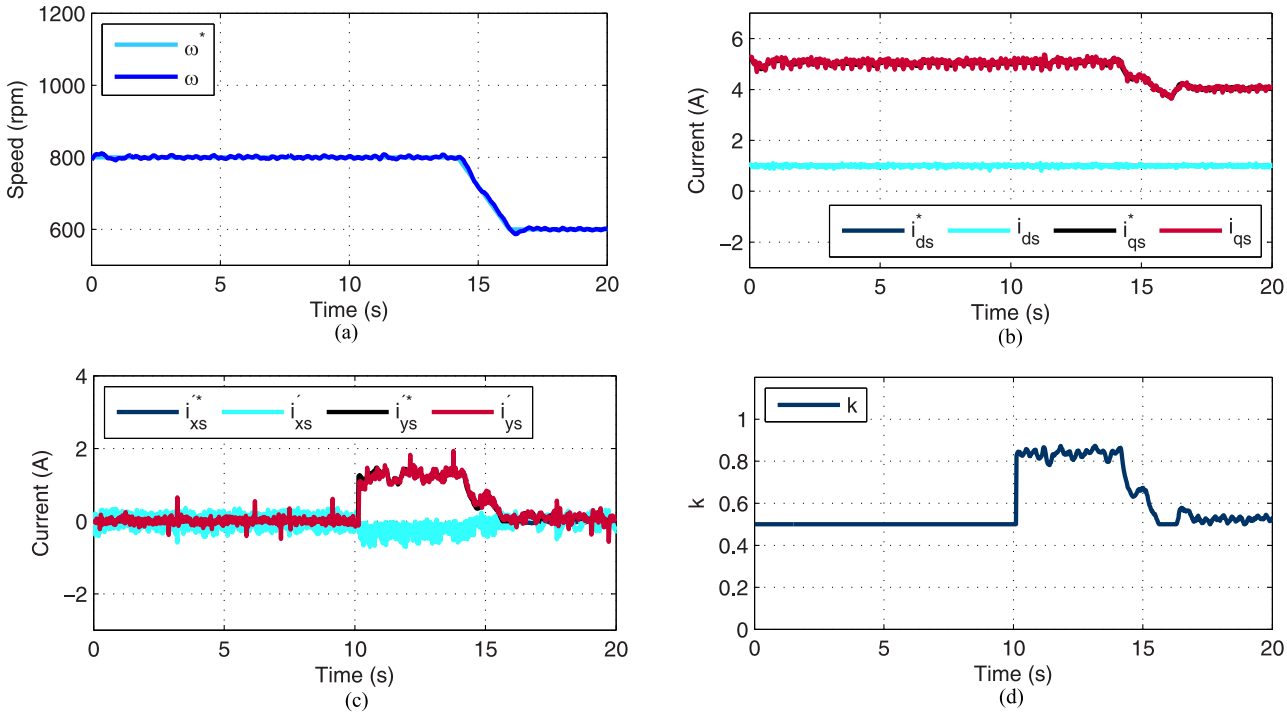

Fig. 6. Experimental results in the test with a speed change from 800 to 600 r/min (postfault). From top to bottom: motor speed, d–q currents, $x' - y'$ currents, and degree of unbalance k.

are found to be very similar in pre- and postfault situations. However, the regulation of k in postfault situation results in nonzero x'–y' currents [see Fig. 6(c)] that guarantee that the drive operates within the current limits in both VSCs1 and VSCs2.

In the next test the six-phase machine is driven at 700 r/min and is loaded by the dc-machine in prefault situation (see Fig. 7). At $t = 15$ s, the dc-machine is disconnected resulting in a sudden unloading of the six-phase induction motor. The load removal

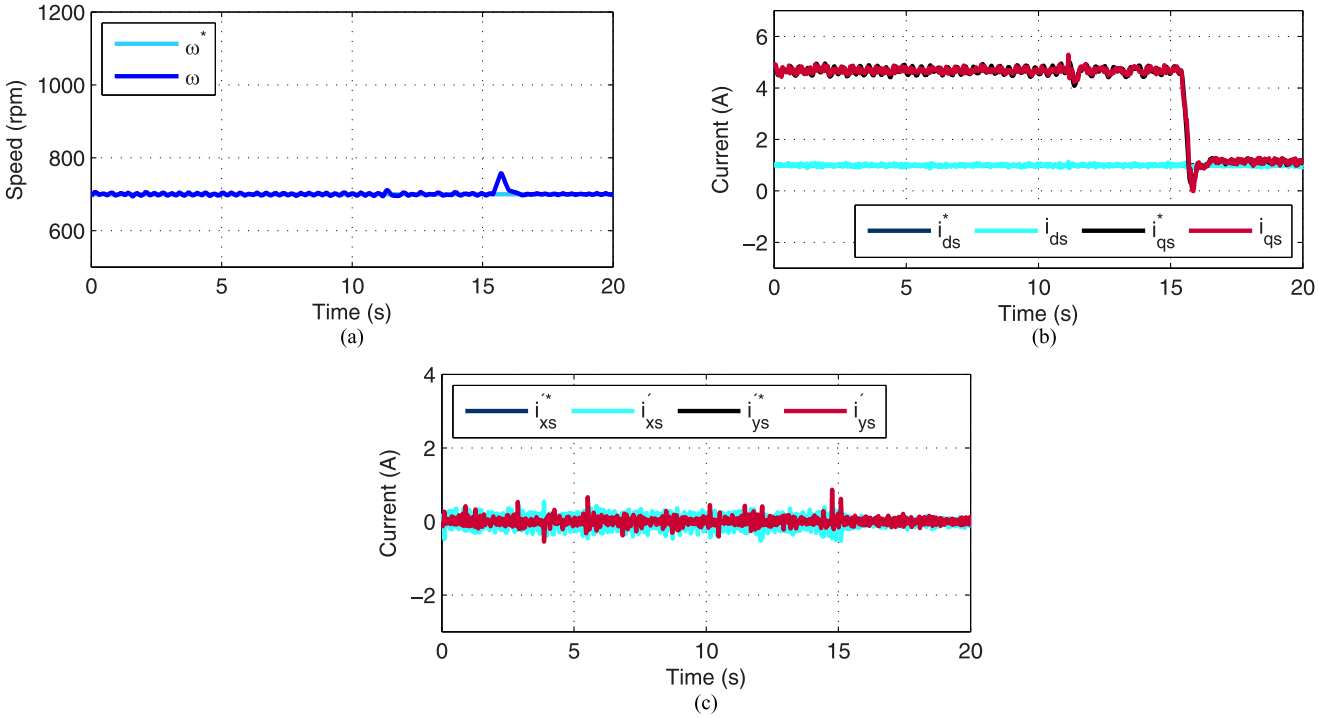

Fig. 7. Experimental results for the load-removal transient at 700 r/min (prefault). From top to bottom: motor speed, d–q currents, and $x' - y'$ currents.

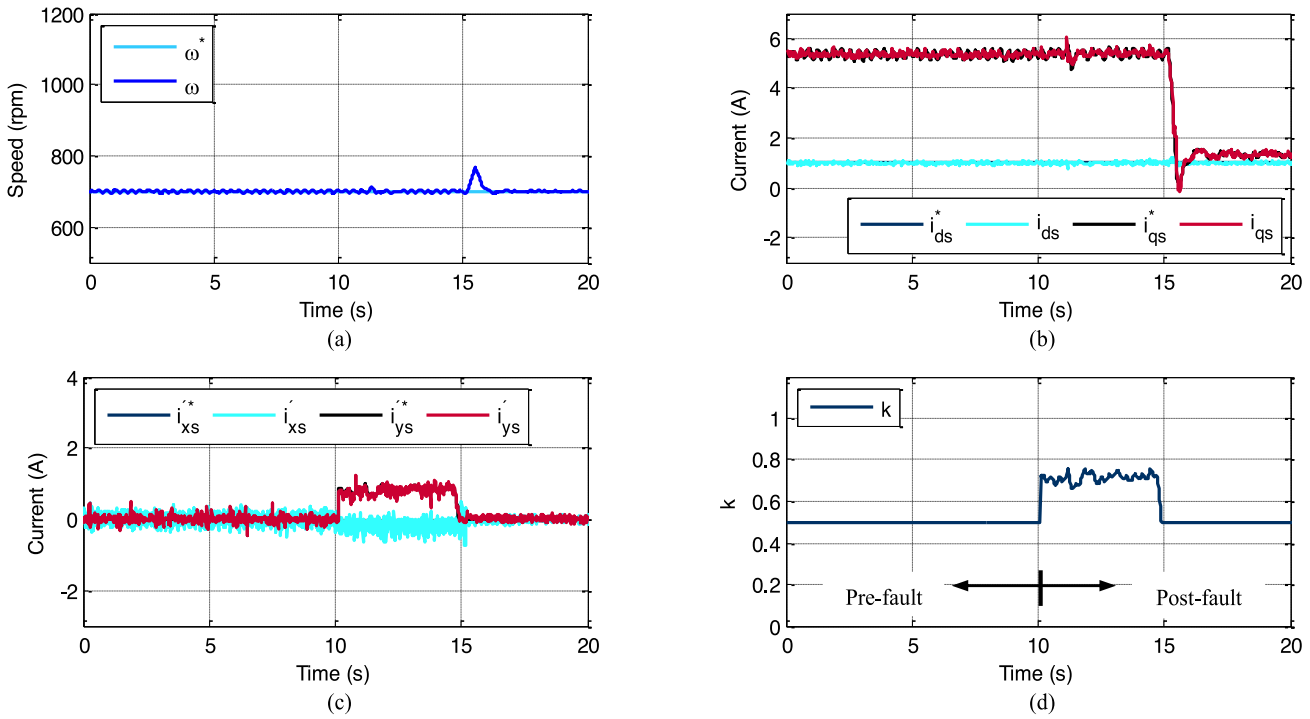

Fig. 8. Experimental results for the load-removal transient at 700 r/min (postfault). From top to bottom: motor speed, d–q currents, $x' - y'$ currents, and degree of unbalance k.

causes a short overshoot of the motor speed [see Fig. 7(a)], but the quick decrease of the q-current [see Fig. 7(b)] decelerates the machine and returns the speed to the reference value. The d current is maintained at 1 A, and the x'–y' currents are controlled to zero [see Fig. 7(c)], showing a good decoupling without any of the sudden unloading. The same test is repeated but including the fault occurrence control at $t = 10$ s (see Fig. 8). The test shows that the value of k is initially increased in postfault situation because the modulus of the d–q currents is over the threshold set in the controller ($|i_{\mathrm{dqs}}| = 4$ A). Nevertheless, when the machine

is unloaded ($t = 15$ s), the unbalanced operation is no longer needed because the balanced operation can generate the required torque. At this point, the value of k is quickly reduced to 0.5 to operate in balanced mode [see Fig. 7(d)]. This is reflected in the x'–y' current references that are regulated back to zero when the machine is unloaded and the imbalance is no longer needed [see Fig. 7(c)]. It must be emphasized here that the unbalanced operation is only desirable when the balanced operation is not feasible, because the nonzero x'–y' currents that are required to provoke the imbalance result in higher copper losses.

Figs. 4 and 8 show that the postfault unbalanced operation can be obtained both in the steady-state and transient situations. The controller of Fig. 2(c) regulates the degree of imbalance k to allow balanced operation when possible (low-torque region) and gradually increases the unequal current sharing when the additional torque is required (up to the limit set by the rated current at $k = 1$).

VI. Conclusion

This study has analyzed different topologies of full-power multiphase energy conversion system using parallel converter supply. The fault-tolerant capability in unbalanced mode of operation has been addressed for the first time in this study, deriving the postfault current references and proposing a new controller that keeps machine currents within postfault ratings. The main conclusion from this study is that it is possible to obtain additional torque/power in six-phase energy conversion systems with parallel converters if some degree of imbalance in the current sharing between the two sets of three-phase windings is allowed. This current sharing can be regulated by proper control of the x–y currents, increasing the α–β current by 50% that results in 225% additional torque/power in the electrical drive for a given slip and frequency The regulation of these nonzero x–y currents can be performed by simple PI controllers in a reference frame with an antisynchronous rotation that eventually results in constant values of the x'–y' references. The controller that regulates the degree of imbalance permits balanced operation in the low-torque region and variable degree of imbalance when the torque is increased, thus achieving minimum copper losses and low dc-link voltage imbalance in cascaded topologies. The imbalance forced by the suggested controller sets an upper limit to ensure that the currents are within acceptable values in both the faulted and healthy sets of three-phase windings. The suggested fault-tolerant mode of operation is feasible in topologies with independent BTB modules as well as in cascaded topologies with a series connection of the machine-side converters and a single grid-side converter.

References

[1] B. Wu, Y. Lang, N. Zargari, and S. Kouro, *Power Conversion and Control of Wind Energy Systems*. Hoboken, NJ, USA: IEEE Press/Wiley, 2011.

[2] M. Liserre, R. Cárdenas, M. Molinas, and J. Rodríguez, "Overview of multi-MW wind turbines and wind parks," *IEEE Trans. Ind. Electron.*, vol. 58, no. 4, pp. 1081–1095, Apr. 2011.

[3] F. Blaabjerg and K. Ma, "Future on power electronics for wind turbine systems," *IEEE J. Emerg. Sel. Topics Power Electron.*, vol. 1, no. 3, pp. 139–152, Sep. 2013.

[4] H. S. Che, W. P. Hew, N. A. Rahim, E. Levi, M. Jones, and M. J. Duran, "A six-phase wind energy induction generator system with series-connected DC-links," in *Proc. IEEE Power Electr. Distrib. Generation Syst.*, 2012, pp. 26–33.

[5] E. Jung, H. Yoo, S. Sul, H. Choi, and Y. Choi, "A nine-phase permanent-magnet motor drive system for an ultrahigh-speed elevator," *IEEE Trans. Ind. Appl.*, vol. 48, no. 3, pp. 987–995, May–Jun. 2012.

[6] Gamesa Technological Corporation S.A. (2014). *Gamesa 5.0 MW* [Online]. Available: http://www.gamesacorp.com/recursos/doc/productos-servicios/aerogeneradores/catalogo-g10x-45mw.pdf

[7] H. S. Che, M. J. Duran, E. Levi, M. Jones, W. P. Hew, and N. A. Rahim, "Postfault operation of an asymmetrical six-phase induction machine with single and two isolated neutral points," *IEEE Trans. Power Electron.*, vol. 29, no. 10, pp. 5406–5416, Oct. 2014.

[8] M. J. Duran, S. Kouro, B. Wu, E. Levi, F. Barrero, and S. Alepuz, "Six-phase PMSG wind energy conversion system based on medium-voltage multilevel converter," in *Proc. Eur. Conf. Power Electr.* and *EPE*, pp. 1–10, CD-ROM, 2011.

[9] H. S. Che, E. Levi, M. Jones, M. J. Duran, W. P. Hew, and N. A. Rahim, "Operation of a six-phase induction machine using series-connected machine-side converters," *IEEE Trans. Ind. Electron.*, vol. 61, no. 1, pp. 164–176, Jan. 2014.

[10] S. S. Gjerde, P. K. Olsen, K. Ljokelsoy, and T. M. Undeland, "Control and fault handling in a modular series-connected converter for a transformerless 100 kV low-weight offshore wind turbine," *IEEE Trans. Ind. Appl.*, vol. 50, no. 2, pp. 1094–1105, Mar.-Apr. 2014.

[11] X. Yuan, J. Chai, and Y. Li, "A transformer-less high-power converter for large permanent magnet wind generator systems," *IEEE Trans. Sustainable Energy*, vol. 3, no. 3, pp. 318–329, Jul. 2012.

[12] E. Levi, "Multiphase electric machines for variable-speed applications," *IEEE Trans. Ind. Electron.*, vol. 55, no. 5, pp. 1893–1909, May 2008.

[13] E. Levi, R. Bojoi, F. Profumo, H. Toliyat, and S. Williamson, "Multiphase induction motor drives—A technology status review," *IET Electric Power Appl.*, vol. 1, no. 4, pp. 489–516, Jul. 2007.

[14] L. Zarri, M. Mengoni, Y. Gritli, A. Tani, F. Filippetti, G. Serra, and D. Casadei, "Detection and localization of stator resistance dissymmetry based on multiple reference frame controllers in multiphase induction motor drives," *IEEE Trans. Ind. Electron.*, vol. 60, no. 8, pp. 3506–3518, Aug. 2013.

[15] M. Salehifar, R. S. Arashloo, J. M. Moreno-Equilaz, V. Sala, and L. Romeral, "Fault detection and fault tolerant operation of a five phase PM motor drive using adaptive model identification approach," *IEEE J. Emerg. Sel. Topics Power Electron.*, vol. 2, no. 2, pp. 212–223, Jun. 2014.

[16] X. Kestelyn and E. Semail, "A vectorial approach for generation of optimal current references for multiphase permanent-magnet synchronous machines in real time," *IEEE Trans. Ind. Electron.*, vol. 58, no. 11, pp. 5057–5065, Nov. 2011.

[17] N. Bianchi, S. Bolognani, and M. D. Pré, "Strategies for the fault-tolerant current control of a five-phase permanent-magnet motor," *IEEE Trans. Ind. Appl.*, vol. 43, no. 4, pp. 960–970, Jul.-Aug. 2007.

[18] A. S. Abdel-Khalik, M. I. Masoud, S. Ahmed, and A. Massoud, "Calculation of derating factors based on steady-state unbalanced multiphase induction machine model under open phase(s) and optimal winding currents," *Electric Power Syst. Res.*, vol. 106, pp. 214–225, Jan. 2014.

[19] H. Guzmán, M. J. Duran, F. Barrero, B. Bogado, and S. Toral, "Speed control of five-phase induction motors with integrated open-phase fault operation using model-based predictive current control techniques," *IEEE Trans. Ind. Electron.*, vol. 61, no. 9, pp. 4474–4484, Sep. 2014.

[20] H. Guzmán, F. Barrero, and M. J. Duran, "IGBT-gating failure effect on a fault-tolerant predictive current controlled 5-phase induction motor drive," *IEEE Trans. Ind. Electron.*, vol. 62, no. 1, pp. 15–20, Jan. 2015.

[21] A. Tani, M. Mengoni, L. Zarri, G. Serra, and D. Casadei, "Control of multiphase induction motors with an odd number of phases under open-circuit phase faults," *IEEE Trans. Power Electron.*, vol. 27, no. 2, pp. 565–577, Feb. 2012.

[22] A. Mohammadpour, S. Sadeghi, and L. Parsa, "A generalized fault-tolerant control strategy for five-phase PM motor drives considering star, pentagon, and pentacle connections of stator windings," *IEEE Trans. Ind. Electron.*, vol. 61, no. 1, pp. 63–75, Jan. 2014.

[23] A. Mohammadpour and L. Parsa, "A unified fault-tolerant current control approach for five-phase PM motors with trapezoidal back EMF under different stator winding connections," *IEEE Trans. Power Electron.*, vol. 28, no. 7, pp. 3517–3527, Jul. 2013.

[24] F. Betin and G. A. Capolino, "Shaft positioning for six-phase induction machines with open phases using variable structure control," *IEEE Trans. Ind. Electron.*, vol. 59, no. 6, pp. 2612–2620, Jun. 2012.
[25] M. A. Fnaiech, F. Betin, G. A. Capolino, and F. Fnaiech, "Fuzzy logic and sliding-mode controls applied to six-phase induction machine with open phases," *IEEE Trans. Ind. Electron.*, vol. 57, no. 1, pp. 354–364, Jan. 2010.
[26] Y. Song and B. Wang, "Survey on reliability of power electronic systems," *IEEE Trans. Power Electron.*, vol. 28, no. 1, pp. 591–604, Jan. 2013.
[27] Z. Xiang-Jun, Y. Yongbing, Z. Hongtao, L. Ying, F. Luguang, and Y. Xu, "Modelling and control of a multi-phase permanent magnet synchronous generator and efficient hybrid 3L-converters for large direct-drive wind turbines," *IET Electr. Power Appl.*, vol. 6, no. 6, pp. 322–331, 2011.
[28] I. Gonzalez, M. J. Duran, H. S. Che, E. Levi, and F. Barrero, "Fault-tolerant control of six-phase induction generators in wind energy conversion systems with series–parallel machine-side converters," in *Proc. IEEE Ann. Conf. Ind. Electr. Soc.*, 2013, pp. 5274–5279.
[29] I. Gonzalez, M. J. Duran, H. S. Che, E. Levi, and J. A. Aguado, "Fault-tolerant efficient control of six-phase induction generators in wind energy conversion systems with series–parallel machine-side converters," in *Proc. Power Electron. Mach. Drives Conf. PEMD*, pp. 1–6, CD-ROM, 2014.
[30] Y. Zhao and T. A. Lipo, "Space vector PWM control of dual three-phase induction machine using vector space decomposition," *IEEE Trans. Ind. Appl.*, vol. 31, no. 5, pp. 1100–1109, Sep.-Oct. 1995.
[31] C. Ditmanson, P. Hein, S. Kolb, J. Mölck, and S. Bernet, "A new modular flux-switching permanent-magnet drive for large wind turbines," *IEEE Trans. Ind. Appl.*, vol. 50, no. 6, pp. 3787–3794, Nov.-Dec. 2014.
[32] H. S. Che, M. J. Duran, W. P. Hew, N. A. Rahim, E. Levi, and M. Jones, "Dc-link voltage balancing of six-phase wind energy systems with series-connected machine-side converters and NPC grid-side converter," in *Proc. IEEE Ann. Conf. Ind. Electr. Soc.*, 2012, pp. 3541–3546.
[33] H. S. Che, E. Levi, M. Jones, W. P. Hew, and N. A. Rahim, "Current control methods for an asymmetrical six-phase induction motor drive," *IEEE Trans. Power Electron.*, vol. 29, no. 10, pp. 5406–5416, Jan. 2014.
[34] M. Jones, S. N. Vukosavic, D. Dujic, and E. Levi, "A synchronous current control scheme for multiphase induction motor drives," *IEEE Trans. Energy Conver.*, vol. 24, no. 4, pp. 860–868, Dec. 2009.
[35] H. Guzmán, M. J. Duran, F. Barrero, L. Zarri, B. Bogado, I. González, and M.R. Arahal, "Comparative study of predictive and resonant controllers in fault-tolerant five-phase induction motor drives," *IEEE Trans. Ind. Electron.*, DOI: 10.1109/TIE.2015.2418732.
[36] Y. Hu, Z. Zhu, and K. Liu, "Current control for dual three-phase permanent magnet synchronous motors accounting for current unbalance and harmonics," *IEEE J. Emerg. Sel. Topics Power Electron.*, vol. 2, no. 2, pp. 272–284, Jun. 2014.
[37] A. Yepes, J. A. Riveros, J. Doval-Gandoy, F. Barrero, O. Lopez, B. Bogado, M. Jones, and E. Levi, "Parameter identification of multiphase induction machines with distributed windings—Part 1: Sinusoidal excitation methods," *IEEE Trans. Energy Conver.*, vol. 27, no. 4, pp. 1056–1066, Dec. 2012.
[38] J. A. Riveros, A. Yepes, F. Barrero, J. Doval-Gandoy, B. Bogado, O. Lopez, M. Jones, and E. Levi, "Parameter identification of multiphase induction machines with distributed windings—Part 2: Time-domain techniques," *IEEE Trans. Energy Conver.*, vol. 27, no. 4, pp. 1067–1077, Dec. 2012.

Ignacio Gonzalez-Prieto was born in Malaga, Spain, in 1987. He received the Ind. Eng. and the M.Sc. degrees from the University of Malaga, Malaga, in 2012 and 2013, respectively. He is currently working toward the Ph.D. degree in the Department of Electronic Engineering, University of Seville, Seville, Spain.

His current research interests include multiphase machines, wind energy systems, and electrical vehicles.

Mario J. Duran was born in Bilbao, Spain, in 1975. He received the M.Sc. and Ph.D. degrees in electrical engineering from the University of Málaga, Malaga, Spain, in 1999 and 2003, respectively.

He is currently an Associate Professor with the Department of Electrical Engineering, University of Málaga. His current research interests include modeling and control of multiphase drives and renewable energies conversion systems.

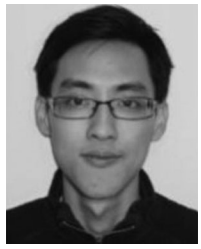

H. S. Che received the B.Eng. degree and the Ph.D. degree under the LJMU-UM dual Ph.D. program from the University of Malaya, Kuala Lumpur, Malaysia, in 2009 and 2013, respectively.

He is currently with the University of Malaya. His current research interests include in the area of multiphase machines and drives, power electronics converters, and renewable energy.

Dr. Che is the sole recipient of the 2009 Kouk Foundation Ph.D. Scholarship.

Emil Levi (S'89–M'92–SM'99–F'09) received the M.Sc. and the Ph.D. degrees in electrical engineering from the University of Belgrade, Belgrade, Yugoslavia, in 1986 and 1990, respectively.

From 1982 to 1992, he was with the Department of Electrical Engineering, University of Novi Sad. He joined Liverpool John Moores University, Merseyside, U.K., in May 1992, where he has been the Professor of Electric Machines and Drives since September 2000..

Dr. Levi is currently the Editor-in-Chief of the *IET Electric Power Applications*. He was a Co-Editor-in-Chief of the IEEE TRANSACTIONS ON INDUSTRIAL ELECTRONICS in the 2009–2013 period and an Editor of the IEEE TRANSACTIONS ON ENERGY CONVERSION. He is the recipient of the Cyril Veinott Award of the IEEE Power and Energy Society for 2009 and the Best Paper award of the IEEE TRANSACTIONS ON INDUSTRIAL ELECTRONICS for 2008. In 2014, he received the "Outstanding Achievement Award" from the European Power Electronics (EPE) Association.

Mario Bermúdez was born in Malaga, Spain, in 1987. He received the Ind.Eng. degree from the University of Málaga, Malaga, Spain, in 2014. He is currently working toward the Ph.D. degree in the Electronic Engineering Department, University of Seville, Seville, Spain.

His current research interests include modeling and control of multiphase drives, DSP-based systems, and electrical vehicles.

Federico Barrero (M 04–SM 05) received the M.Sc. and the Ph.D. degrees in electrical and electronic engineering from the University of Seville, Seville, Spain, in 1992 and 1998, respectively.

In 1992, he joined the Electronic Engineering Department, University of Seville, where he is currently an Associate Professor.

Dr. Barrero received the Best Paper Awards from the IEEE TRANSACTIONS ON INDUSTRIAL ELECTRONICS for 2009 and from the IET Electric Power Applications for 2010–2011.